Experimental and theoretical studies of a coaxial free-electron maser based on two-dimensional distributed feedback

I. V. Konoplev,* A. W. Cross, A. D. R. Phelps, W. He, K. Ronald, C. G. Whyte, C. W. Robertson, and P. MacInnes
SUPA, Department of Physics, University of Strathclyde, Glasgow G4 0NG, United Kingdom

N. S. Ginzburg, N. Yu. Peskov, A. S. Sergeev, and V. Yu. Zaslavsky
Institute of Applied Physics, Russian Academy of Sciences, Nizhny Novgorod. 603950 Russia

M. Thumm
Institut für Höchstfrequenztechnik und Elektronik, Universität Karlsruhe, Karlsruhe D-76131, Germany
and Forschungszentrum Karlsruhe, Institut für Höchleistungsimpuls- und Mikrowellentechnik, Karlsruhe D-76021, Germany
(Received 23 January 2007; published 30 November 2007)

The first operation of a coaxial free-electron maser (FEM) based on two-dimensional (2D) distributed feedback has been recently observed. Analytical and numerical modeling, as well as measurements, of microwave radiation generated by a FEM with a cavity defined by coaxial structures with a 2D periodic perturbation on the inner surfaces of the outer conductor were carried out. The two-mirror cavity was formed with two 2D periodic structures separated by a central smooth section of coaxial waveguide. The FEM was driven by a large diameter (7 cm), high-current (500 A), annular electron beam with electron energy of 475 keV. Studies of the FEM operation have been conducted. It has been demonstrated that by tuning the amplitude of the undulator or guide magnetic field, modes associated with the different band gaps of the 2D structures were excited. The Ka-band FEM generated 15 MW of radiation with a 6% conversion efficiency, in good agreement with theory.

DOI: 10.1103/PhysRevE.76.056406 PACS number(s): 52.59.Rz, 42.55.Tv, 84.40.Ik, 41.60.Cr

I. INTRODUCTION

In recent years the demand for high power masers operating at sub-GW and GW powers in the frequency range from 30 GHz to 300 GHz has significantly increased [1–3]. For instance, such masers are required for plasma heating, new accelerator facilities, remote sensing, and material science. Interest has also been shown in masers capable of producing coherent radiation in the THz frequency range [4–6]. Masers operating in both the 30 GHz–300 GHz and THz frequency range suffer from a problem associated with the high electromagnetic (EM) field power density inside the interaction space, where the energy exchange between the EM field and the active medium takes place. The power density can become large, leading to breakdown inside the interaction space of a maser. The use of two-dimensional (2D) distributed feedback has been proposed [7] to circumvent the problem by providing spatial and temporal coherence of the radiation from a large size (in comparison with the operating wavelength) active medium [8–10]. Previous studies [11,12] have demonstrated that the use of a 2D lattice allows one to observe 2D distributed feedback via wave scattering on the periodic perturbations. The 2D lattice can be obtained via machining doubly periodic corrugations on the side walls of the planar, or coaxial waveguides. On such a corrugation a mutual scattering of the electromagnetic energy fluxes propagating in the forward, backward, and transverse directions takes place. As a result the transverse electromagnetic energy fluxes synchronize the radiation from the different parts of a large size electron beam. The numerical simulations conducted earlier had demonstrated [8–10] that installation of such structures inside the interaction space allows the transverse size of the interaction space, the total electron beam power, and the output power all to be increased while still maintaining the electron beam current density and radiation density per unit transverse size below the breakdown threshold. It was also shown theoretically that the feedback mechanism ensures effective mode selection in an oversized cavity.

In this paper a free-electron maser (FEM) based on a coaxial cavity utilizing 2D distributed feedback has been studied theoretically and experimentally. In Sec. II the analytical and numerical models of the 2D coaxial structures used in the experimental studies of the FEM are presented. The properties of the structures such as the reflection and the transmission coefficients are analyzed and the EM field evolution inside the structures is considered. The numerical simulations have been conducted and results observed are compared with the analytical predictions. In Sec. II the results of the theoretical studies are also compared with the experimental data. In Sec. III the two-mirror cavity formed by two 2D coaxial periodic structures (input and output mirrors) with smooth coaxial waveguide in between is studied and using the data observed in Sec. II the two-mirror cavity for the FEM experiment is designed. The numerical simulations of the operation of the FEM based on such a cavity are conducted. Also to optimize the FEM parameters such as the guide magnetic field amplitude, the period of the undulator, and the amplitude of the undulator field, the simulation of the single-pass FEM in the self-amplification of spontaneous emission (SASE) regime has been conducted and the results are presented. The theoretical studies of excitation, build-up of oscillations, and operation of the FEM based on a 2D

*Author to whom correspondence should be addressed. FAX: +44-141-5522891. acp96115@strath.ac.uk

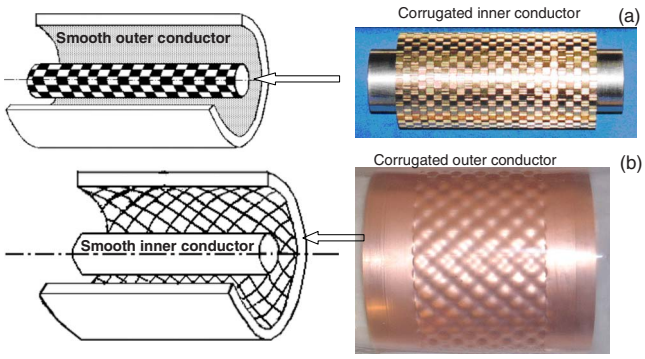

FIG. 1. (Color online) The schematics and photographs of the 2D Bragg structures with corrugated (a) inner and (b) outer conductors.

Bragg two-mirror cavity are also conducted in this Sec. III. In Sec. IV the experimental setup built to conduct the FEM experiments is discussed. The main parameters of the electron beam produced by the high-current accelerator (HCA) used to drive the FEM are presented. Numerical simulations of the HCA operation have been conducted and compared with the experimental data. Also in Sec. IV, the first measurements of microwave radiation from a coaxial FEM based on a two-mirror cavity formed by 2D Bragg structures are presented. An output power of ~15 MW corresponding to an efficiency of ~6% was measured. The mode pattern of the output radiation from the horn antenna has also been measured. The frequency of the output radiation was also analyzed, first by using the cutoff filters and then more accurately using a heterodyne frequency diagnostic. The results of the output signal spectrum studies are shown and discussed. In the last section the conclusions are presented and future work and development of the experiment are discussed.

II. STUDY OF COAXIAL 2D BRAGG STRUCTURE

A coaxial "ideal" 2D structure consists of two conductors of radii r_{in}, r_{out}, length l_z, having a small depth corrugation of either the inner [Fig. 1(a)] or the outer [Fig. 1(b)] conductor in the form

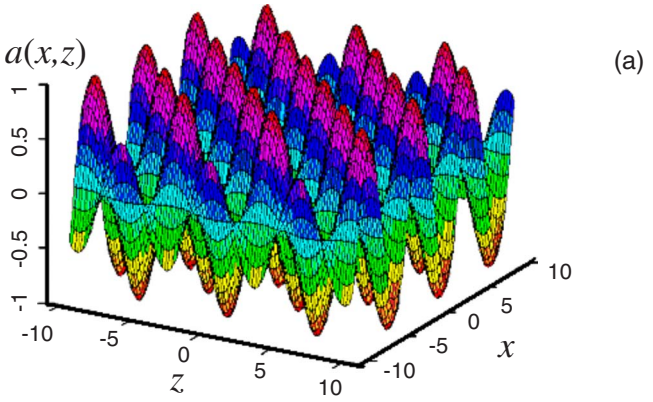

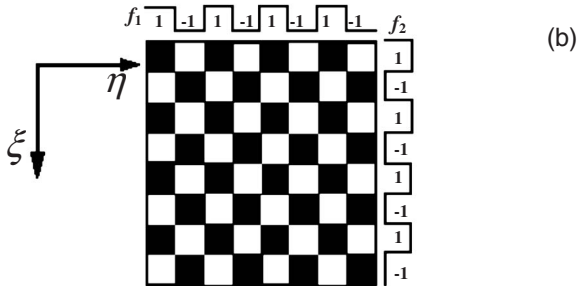

FIG. 2. (Color online) The schematics of the 2D periodic perturbations with an (a) "ideal" sinusoidal pattern and (b) square wave "chessboard" pattern.

$$a = r_{\text{in,out}} + a_1 \cos(\bar{k}_z z)\cos(\bar{m}\varphi), \tag{1}$$

where a_1 is the corrugation depth, $\bar{k}_z = 2\pi/d_z$, d_z is the period of the perturbation over the z coordinate, and $\bar{m}$ is the number of perturbation variations over the azimuthal coordinate [12]. It has been shown previously [11,12] that an "ideal" lattice [Fig. 2(a)] can be substituted with "square" wave perturbations having "chessboard" patterns [Fig. 2(b)] of the waveguide surface. The corrugation with a "chessboard" pattern can be obtained by assembling gears of a half-period width, or by using micromachining techniques. In this case 2D corrugated surfaces can be described as the product of the two functions [11], $a = f_1(\bar{k}_\xi \xi) f_2(\bar{k}_\eta \eta)$, where

$$f_i(\zeta) = \begin{cases} -1, & 0 < \zeta < d_\zeta/2 \\ 1, & d_\zeta/2 < \zeta < d_\zeta, \end{cases} \quad \zeta \text{ is the variable, } i = 1,2 \text{ and } d_\varsigma \text{ is the period of the functions,}$$

$$f_i(\zeta + d_\zeta) = f_i(\zeta).$$

In the present experiments the properties of both 2D lattices have been studied and analyzed. We assume (taking into account the actual parameters of these experiments) that the radii r_{in}, r_{out} greatly exceed the distance between the conductors $a_0 = r_{out} - r_{in}$ and the radiation wavelength, $r_{in,out} \gg a_0$ and $r_{in,out} \gg \lambda$. Under these conditions the dispersion equation for the eigenwaves of the coaxial waveguide can be reduced to the following form [13]:

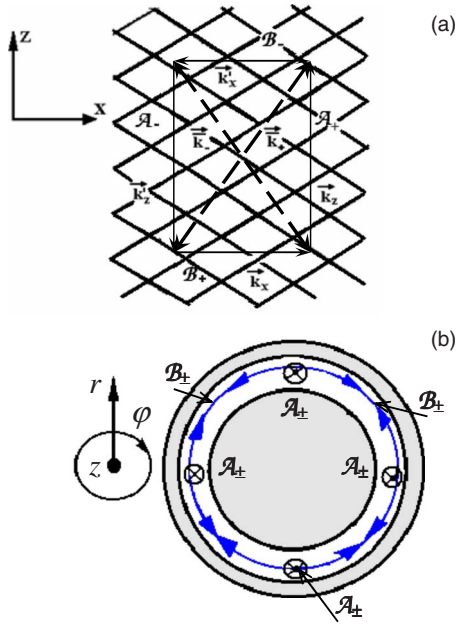

FIG. 3. (Color online) (a) Schematic diagram of the 2D feedback loop formation via partial wave coupling on the surface of "ideal" 2D lattice. (b) The schematic diagram of the partial wave propagation inside the 2D coaxial Bragg structure with the "ideal" corrugation.

$$k^2 = \frac{\omega^2}{c^2} \cong k_z^2 + k_\perp^2, \tag{2}$$

where ω is the wave frequency, c is the speed of light, k_z is the longitudinal wave number, $k_\perp^2 = k_r^2 + k_\varphi^2$, $k_\varphi = M/r_0$ is the azimuthal wave number, $r_0 = (r_{\text{in}} + r_{\text{out}})/2$, $k_r = p\pi/a_0$ is the radial wave number, and M and p are the azimuthal and radial variation indices, respectively. The dispersion equation (2) is similar to the equation that describes the eigenwaves of the planar waveguide. This allows one to neglect the small curvature of the cavity surface and to adopt the planar coordinate system by introducing the new transverse coordinate $x = r_0 \times \varphi$, which enables k_x to be used instead of k_φ, i.e., $k_x \equiv k_\varphi$.

The field inside the 2D structure can be presented in the form of four coupled waves: $A_\pm$ propagating in the $\pm z$ directions and $B_\pm$ are near cutoff waves "propagating" in the $\pm x$ directions [Fig. 3(a)],

$$\vec{E} = \text{Re}(\{\vec{E}_b^0(r)[B_+(x,z)e^{-ik_x x} + B_-(x,z)e^{ik_x' x}] + \vec{E}_a^0(r)[A_+(x,z)e^{-ik_z z} + A_-(x,z)e^{ik_z' z}]\}e^{i\omega t}). \tag{3}$$

Here $A_\pm(x,z)$, $B_\pm(x,z)$ are slowly varying functions of the x and z coordinates, k_x, k_x' and k_z, k_z' are the azimuthal and longitudinal wave numbers of the partial waves B_+, B_- and A_+, A_-, respectively, and $E_{a,b}^0(r)$ are functions describing the spatial wave profile along the r coordinate, which coincides with one of the eigenmodes of the coaxial waveguide.

The 2D lattice eigenvectors can be represented as $\vec{\bar{k}}_\pm = \bar{k}_x \vec{x}_0 \pm \bar{k}_z \vec{z}_0$ where $\vec{x}_0$ and $\vec{z}_0$ are the unit vectors along the x and z coordinates and $\bar{k}_x$, $\bar{k}_z$ are the amplitudes of the projections of the lattice eigenvectors $\vec{\bar{k}}_\pm$ on the axes x and z. In Fig. 3(a) the partial wave A_+ propagating in the $+z$ direction is scattered into waves $B_\pm$ propagating in the transverse $\pm x$ directions and scattering into waves $A_\pm$, which ensures that the two-dimensional feedback loop $A_+ \leftrightarrow B_\pm \leftrightarrow A_- \leftrightarrow B_\pm \leftrightarrow A_+$ is completed. In Fig. 3(b) the schematic of the partial wave propagation in the coaxial structure is presented. To obtain an efficient coupling of the partial waves $A_\pm \leftrightarrow B_\pm$ the following Bragg resonance conditions [10–12] should be satisfied for each pair of coupled waves:

$$\vec{k}_z - \vec{k}_x = \vec{\bar{k}}_-, \quad \vec{k}_z' - \vec{k}_x' = -\vec{\bar{k}}_-, \quad \vec{k}_z - \vec{k}_x' = \vec{\bar{k}}_+, \quad \vec{k}_z' - \vec{k}_x = -\vec{\bar{k}}_+. \tag{4}$$

Taking into account that the 2D feedback loop can only be obtained when conditions (4) are fulfilled simultaneously and assuming that the structures of the forward and backward waves coincide with the structure of the transverse electromagnetic waves (TEM) wave of the coaxial waveguide, the four partial waves undergo coupling on the 2D lattice if

$$k_z = k_z' \cong \bar{k}_z, \quad k_x = k_x' \cong \bar{k}_x, \quad \text{and} \quad |k_z| \approx |k_\perp'|, \tag{5}$$

where $k_\perp'$ is the transverse wave number of the partial waves $B_\pm$. The last condition in (5) follows from the condition that the structures of waves $B_\pm$ should be close to those of near cutoff waves of the waveguide.

To simulate the field scattering inside the coaxial structure with 2D periodic perturbations such that conditions (5) can be met the three-dimensional (3D) particle-in-cell (PIC) code MAGIC has been used. In Fig. 4 the snapshots of the profiles of the propagating waves $A_\pm$ [Fig. 4(a)] and near cutoff waves $B_\pm$ at the cross section are shown for the 2D Bragg structures with corrugated inner [Fig. 4(b)] and outer [Fig. 4(c)] conductors. In both cases the period of the corrugations was $d_z = 8$ mm while the number of azimuthal variations in the first case was $\bar{m} = 24$ and in the second case was $\bar{m} = 28$. In Figs. 4(b) and 4(c) the cross sections correspond to the center of the 2D structures, while the cross section presented in Fig. 4(a) is associated with the input section of the structure. In the simulations the 2D structures have been excited by the TEM wave of the coaxial waveguide. The forward and backward propagating waves had the transverse structure of a TEM wave in the coaxial waveguide [Fig. 4(a)], i.e., the wave has only radial electric and azimuthal magnetic field components. The field components (B_z) observed in simulations and presented in Figs. 4(b) and 4(c) can only be attributed to the near cutoff waves $\text{TE}_{24,1}$ and $\text{TE}_{28,0}$, respectively, of the coaxial waveguide (partial waves $B_\pm$).

It is clear that due to the circular geometry of the system the wave amplitudes should satisfy the cyclic boundary conditions, i.e., $A_\pm(x + l_x, z) = A_\pm(x,z)$, $B_\pm(x + l_x, z) = B_\pm(x,z)$, where $l_x = 2\pi r_0$ is the cavity mean circumference. These conditions allow the partial wave amplitudes $A_\pm(x,z)$, $B_\pm(x,z)$ to be represented by the Fourier series

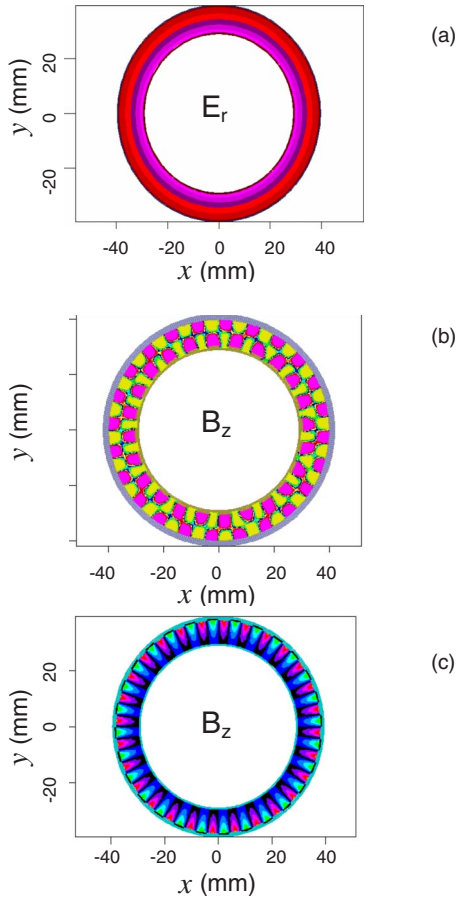

FIG. 4. (Color online) The transverse structure of the (a) radial component of the electric field (E_r) of the wave incident on the structures and the longitudinal component of the magnetic field (B_z) inside the structure with (b) corrugated inner conductor ($\bar{m}=24$); (c) corrugated outer conductor ($\bar{m}=28$).

$$A_{\pm}(x,z)=\sum_{m=-\infty}^{\infty}A_{\pm}^{m}(z)e^{imsx},\quad B_{\pm}(x,z)=\sum_{m'=-\infty}^{\infty}B_{\pm}^{m'}(z)e^{im'sx}, \tag{6}$$

where $s=2\pi/l_x=1/r_0$ and the field evolution corresponds to the evolution of the amplitude of the Fourier series. It is important to note that m and m' in (6) are linked together via conditions (4) [10,11]. As a result the coupled wave equations can be written as [10]

$$B_{+}^{m}+B_{-}^{m}=\frac{-2i\alpha(i\delta+\sigma)(A_{+}^{m}+A_{-}^{m})}{(i\delta+\sigma)^2+s^2m^2}, \tag{7}$$

$$\pm\frac{dA_{\pm}^{m}}{dz}+\frac{2\alpha^2(i\delta+\sigma)}{(i\delta+\sigma)^2+s^2m^2}(A_{+}^{m}+A_{-}^{m})+(i\delta+\sigma)A_{\pm}^{m}=0. \tag{8}$$

Taking this into account the boundary conditions' analytical expressions for the reflection R_m and the transmission T_m coefficients can be obtained as functions of the incident wave's azimuthal index m and wave frequency detuning $\delta=(\omega-\bar{\omega})/c$ from the exact Bragg resonance frequency $\bar{\omega}$,

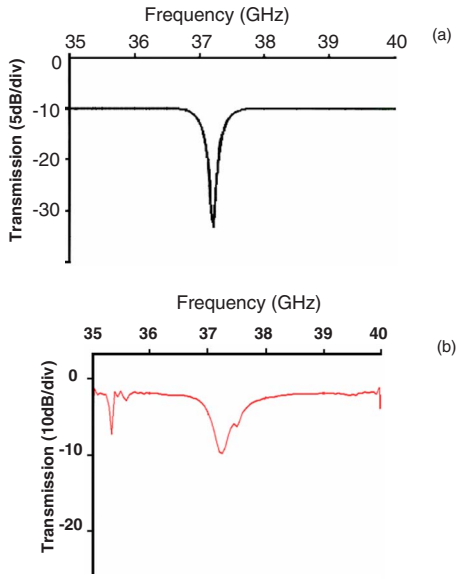

FIG. 5. (Color online) The transmission coefficient through the 2D Bragg structure with corrugated inner conductor observed via (a) analytical expression (6) and (b) 3D numerical simulation of pulse propagation through the structure.

$$R_m=\frac{\lambda_m^2-p_m^2}{q_m[p_m-\lambda_m\cot(\lambda_m l_z)]},$$

$$T_m=\frac{-i\lambda_m}{\sin(\lambda_m l_z)[p_m-i\bar{\lambda}_m\cot(\lambda_m l_z)]}, \tag{9}$$

where

$$q_m=\frac{2\alpha^2\tilde{\delta}}{s^2m^2+\tilde{\delta}^2},\quad p_m=\frac{2\tilde{\delta}\alpha^2}{s^2m^2+\tilde{\delta}^2}+\tilde{\delta}$$

$$\tilde{\delta}=i\delta+\sigma,\quad \lambda_m=-i\tilde{\delta}\sqrt{\frac{4\alpha^2}{\tilde{\delta}^2+s^2m^2}+1},$$

and α is the wave coupling coefficient [10]. Analyzing the expressions obtained we must note that for each mode with index m such a structure provides an effective reflection zone (band gap), inside a frequency interval defined by the condition $\mathrm{Re}(\lambda_m^2)\leq 0$. Let us note that it is possible to find corrugation parameters such that the reflection zones for different modes do not overlap each other, which is very important for obtaining narrow band, mode selective mirrors.

In the present experiments the structures of the partial waves $A_{\pm}$ have been considered to coincide with the structure of the TEM wave. These waves interacting with the 2D lattice are indirectly coupled via the waves $B_{\pm}$ having an azimuthal variation index $M=\pm\bar{m}$ [11]. The dependence of the transmission coefficient of the incident wave A_{+} as a function of frequency predicted by expression (9) is presented in Fig. 5(a). In Fig. 5(b) the theoretical results obtained from the full 3D simulation of the experimental system using the PIC code MAGIC are shown. To observe the results presented in Fig.

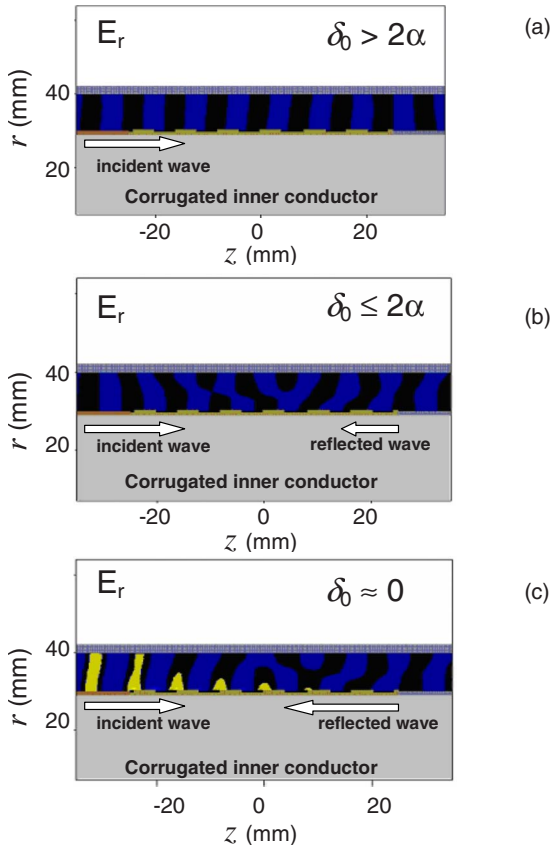

FIG. 6. (Color online) The results of numerical simulations of wave interaction with 2D "square" wave lattice if the wave frequency is (a) far from the Bragg resonance frequency, (b) in the vicinity of the Bragg frequency, and (c) equal to the Bragg frequency.

5(b) the 2D Bragg structure was excited using an amplitude modulated radiation pulse formed by a TEM wave with an initially flat-top spectrum in the frequency range from 35 GHz to 40 GHz. After the radiation pulse passed through the structure the gap in the spectrum associated with partial reflection of the pulse has appeared [Fig. 5(b)]. In Fig. 6 the numerical simulation of the formation of the reflected wave is presented. In Fig. 6(a) the unperturbed propagation of the wave detuned from the Bragg resonance is clear. Gradually shifting the frequency of the wave to the vicinity of the resonance, a weak wave interaction with the structure is observed [Fig. 6(b)]. The reflected wave is formed [Fig. 6(c)], if the wave frequency is close to the resonance.

For further analysis of the properties of the 2D structures an experimental setup to measure the structures' transmission and reflection coefficients was constructed. In Fig. 7 the photographs of the setup are presented. For excitation of the structures a TEM mode of a coaxial waveguide was formed at the input of the Bragg structures. To produce such a wave beam an additional transmission line was designed and constructed, shown in Fig. 7(a). The input of the transmission line was a single-mode, Ka-band rectangular waveguide (7.2 mm × 3.8 mm). The transmission line itself was made from three mode converters, which provide the required mode transformation in the operating frequency band

FIG. 7. (Color online) The photograph of the experimental setup (a) to study the properties of the 2D Bragg structures with corrugated (b) inner conductor and (c) outer conductor.

(30 GHz–40 GHz): from the launched $TE_{0,1}$ wave of single mode rectangular waveguide to the $TE_{1,1}$ wave of a circular waveguide (the first mode converter) then to a $TM_{0,1}$ wave of circular waveguide (the second mode converter) and finally to a TEM wave of a coaxial waveguide (the third mode converter). An additional coaxial slowly up-tapered waveguide horn (opening angle of 3°) of length ~60 cm was used to connect from the converters to the oversized coaxial structure. The output dimensions of the coaxial waveguide at the connection with the Bragg structure were as follows: diameter of the inner conductor of 5.9 cm and outer conductor of 7.9 cm.

The 2D Bragg structures with corrugated inner [Fig. 7(c)] and outer [Fig. 7(b)] conductors have been studied. The 2D lattice for the 2D Bragg structure with corrugated inner conductor has been machined in the form of "square" waves with a "chessboard" pattern [Fig. 7(c)], while the lattice for the structure with a corrugated inner surface of the outer conductor has been machined in the form of "sinusoidal" waves [Fig. 7(b)] which is close to the "ideal" corrugation described by (1). To provide stronger coupling between the partial waves, the 2D structure with a corrugated inner conductor had $\bar{m}=24$ azimuthal variations, while the structure with a corrugated outer conductor had $\bar{m}=28$ variations. Indeed, it is clear from Fig. 4 that the mode $TE_{28,0}$ has the highest field amplitude at the surface of the outer conductor and therefore the coupling between the waves and the lattice will be significantly weaker if these 28 azimuthal variations were to be machined on the outer surface of the inner conductor. The lattice with the "chessboard" pattern had a corrugation depth of 0.8 mm, which corresponds to a coupling coefficient of $\alpha \approx 0.12$ cm^{-1}, while the depth of the sinu-

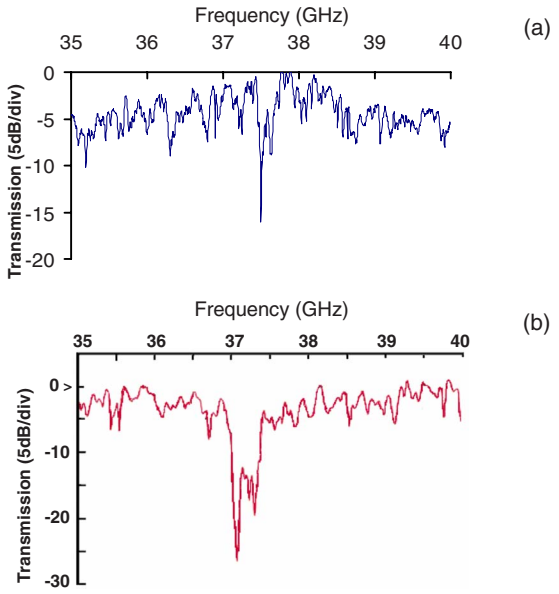

FIG. 8. (Color online) The transmission coefficient measured through the 2D Bragg structures with corrugated (a) outer conductor ($\bar{m}=28$) of length 48 mm and corrugation depth of 1 mm; (b) corrugated inner conductor ($\bar{m}=24$) of length 56 mm and corrugation depth of 1.6 mm.

soidal lattice was 0.5 mm, which corresponds to $\alpha \approx 0.1$ cm^{-1}. The coaxial structures were based on the coaxial waveguide with inner and outer radii of $r_{\text{in}}=2.95$ cm, $r_{\text{out}}=3.90$ cm, respectively. The chessboard and the sinusoidal structures had periods of $d_z=0.804$ cm and $d_z=0.800$ cm, which correspond to the frequencies of the precise resonances (Bragg frequencies) of 37.3 GHz and 37.5 GHz, respectively. The lengths of the structures were 4.8 cm and 5.6 cm, respectively. The parameters of the corrugation were chosen to provide the following wave couplings: $\text{TEM} \leftrightarrow \text{TE}_{24,1} \leftrightarrow \text{TEM}$ and $\text{TEM} \leftrightarrow \text{TE}_{28,0} \leftrightarrow \text{TEM}$. In Figs. 8(a) and 8(b) the transmission coefficients of the 2D Bragg structures as a function of the frequency of the incident wave are presented. Comparing the experimental results (Fig. 8) with the theoretical predictions (Fig. 5), there is evidently good agreement.

III. MODEL OF FEM BASED ON TWO-MIRROR 2D BRAGG CAVITY

Let us study the two-mirror cavity, which consists of two 2D Bragg coaxial structures operating as input and output mirrors, with the regular part of the coaxial waveguide (Fig. 9) situated in between. We assume that the amplitudes of the waves incident upon the resonator are equal to zero, i.e., $A_+^m|_{z=0}=0$, $A_-^m|_{z=l_\Sigma}=0$, where l_Σ is the two-mirror resonator's full length. Assuming the absence of ohmic losses in the regular part of the resonator, the continuity conditions for the partial waves at the boundaries between the mirrors and the regular part can be written as

$$A_+^1(z=l_1)=A_+^2(z=l_1+l_0)e^{-i\delta l_0},$$

$$A_-^1(z=l_1)=A_-^2(z=l_1+l_0)e^{i\delta l_0}, \tag{10}$$

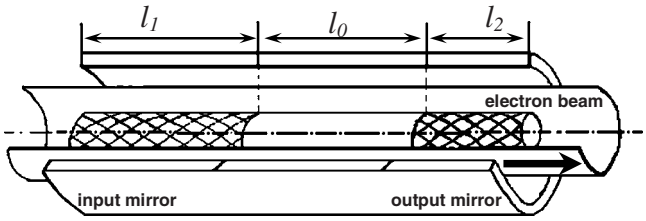

FIG. 9. Schematic diagram of the two-mirror coaxial cavity that is formed by 2D Bragg structures (input and output mirrors of lengths l_1 and l_2) and regular coaxial waveguide of length l_0. The annular electron beam passes between the inner and outer conductors as shown on the diagram.

where l_1, l_1+l_0 are the coordinates of the inside boundaries and δ_0 is replaced with complex δ.

Taking into account (7) and (8) the set of equations to describe the field evolution inside the cavity can be presented in the following form [10]:

$$\pm\frac{dA_\pm^{m,j}}{dz}+\frac{2\alpha^2(i\delta+\sigma)}{(i\delta+\sigma)^2+s^2m^2}(A_+^{m,j}+A_-^{m,j})+(i\delta+\sigma)A_+^{m,j}=0,$$

$$\pm\frac{dA_\pm^{m,0}}{dz}+i\delta A_-^{m,0}=0, \tag{11}$$

where $A_\pm^m$ are the amplitudes of the Fourier terms (6) and $j=1,2$ refers to the first and the second corrugated parts and 0 corresponds to the regular part of the cavity. The solution of (11) with the zero boundary conditions yields the characteristic equation [10]

$$R_1R_2=e^{2i\delta l_0}, \tag{12}$$

where R_1 and R_2 are defined by (9). The imaginary part of complex δ indicates the losses of the eigenmodes in the cavity and defines the eigenmodes' Q factors. Let us find the high Q-factor eigenmodes of the two-mirror resonator, if the parameters of the input and output mirrors are the same except for their lengths. We assume that the output mirror is the shortest one and thus the effective width of its reflection zone is smallest [11] and defines the frequency range of the possible location of the cavity eigenmodes. The solutions of Eq. (12) can be found [10] and the locations and Q factors of the eigenmodes can be described by the following expressions:

$$\text{Re}\ \delta_{m,n}\cong\frac{\pi n}{l_0}+sm, \tag{13}$$

$$Q_{m,n}\cong\frac{\omega l_0}{c[1-|R_1(\text{Re}\ \delta_{mn})R_2(\text{Re}\ \delta_{mn})|]}, \tag{14}$$

where n displays the number of longitudinal field variations along the length of the regular part of the waveguide. As is easy to see from analysis of (14) and (9) the mode with the azimuthal indices $m=0$ and $n=0$ has the highest Q factor, limited only by ohmic losses. It should be noted, we have assumed that the mirrors' lengths are much smaller than the length of the regular part of the system and l_0 (length of the regular part of the resonator) is used in the formulas instead of the full length of the cavity. Comparing the expression for

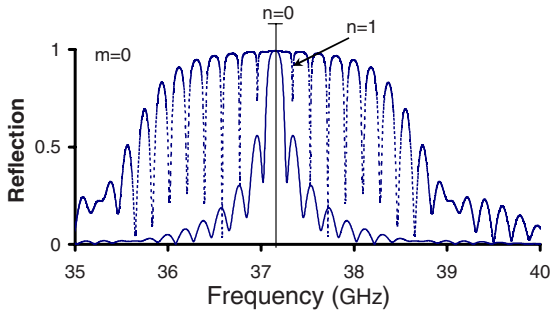

FIG. 10. (Color online) The reflection coefficient through the two-mirror cavity based on 2D Bragg structures for $l_1=10$ cm, $l_2=6$ cm, $l_0=70$ cm, and $\alpha=0.12$ cm^{-1} (dotted line); $\alpha=0.03$ cm^{-1} (solid line).

the eigenmode location and the width of the mirrors' reflection zones one can find a range of the mirror parameters where only one mode ($n=0$) exists inside the reflection zone of the output mirror,

$$\frac{\pi}{l_0} \geq 2\alpha. \tag{15}$$

Thus such a resonator can provide selection over both azimuthal m (see the preceding section) and longitudinal n indices, thus maintaining a single mode operation regime. The position of the eigenmodes can also be found by considering the reflection coefficient from the entire two-mirror cavity [10]. In Fig. 10 the reflection coefficient through the two-mirror cavity used to define the FEM interaction space is presented (dotted line). The locations of the minima of the reflection coefficient coincide with the locations of the eigenmodes. It is important to note that in the approximation considered, the fundamental mode of the cavity ($m=0, n=0$) has an infinite Q factor associated with the diffraction losses and thus cannot be resolved ($\Delta\omega \sim \omega/Q$). However, it is clear from the graph that the presence of many longitudinal modes with a finite, but high, Q factor can be expected. It is important to stress that for the first proof-of-principle experiment the cavity parameters were chosen to ensure the start-up of oscillations and therefore the achievement of perfect spectral purity was outside the scope of the first experiments. Nevertheless, to improve the spectral purity the coupling coefficient (for example) can be decreased, thereby, significantly decreasing the Q factor of the parasitic modes with longitudinal indices above 0, as demonstrated in Fig. 10 (bold line).

Let us now investigate the excitation of the two-mirror 2D Bragg cavity (Fig. 9) by an annular relativistic electron beam. Let us assume that the electron beam is thin and traveling centrally, between the conductors of the coaxial waveguide. Indeed in the experiments the electron beam thickness did not exceed 0.2 cm, while the average beam diameter was 7 cm and the electron beam was aligned to propagate in the middle of the coaxial channel gap between inner and outer conductors. Let us neglect the inhomogeneities of the undulator field (in the experiment such field perturbations did not exceed 10% of the undulator field amplitude), as well as nonuniformities of the beam in both the azimuthal and radial directions. We also take into account that only the A_+ wave is resonant with the electrons moving in the $+z$ direction and that the other partial waves do not interact with the beam. Therefore, only the resonant forward wave A_+ may be amplified by the electron beam. The resonance condition can be written in the form

$$\omega - k_z v_\parallel = \Omega_b, \tag{16}$$

where $v_\parallel=\beta_\parallel c$ is the electron axial velocity, $\Omega_b=2\pi v_\parallel/d_u$ is the bounce-frequency, and d_u is the undulator period. On the grating the wave A_+ scatters into waves $B_\pm$, which propagate in the transverse directions and synchronize (after further transformation into the wave A_+) radiation from different parts of the electron beam. Simultaneously the waves $B_\pm$ scatter into the backward wave A_-, thus forming a feedback cycle (Fig. 2).

The excitation of a 2D two-mirror cavity by the electron beam and the build-up of oscillations can be described by the following system of equations [10]:

$$\left(\frac{\partial}{\partial Z}+\frac{\partial}{\beta_{gr}\partial\tau}\right)\hat{A}_+^j+\sigma\hat{A}_+^j+i\hat{\alpha}(\hat{B}_+^j+\hat{B}_-^j)=\frac{1}{\pi}\int_0^{2\pi}e^{-i\Theta}d\Theta_0,$$

$$\left(-\frac{\partial}{\partial Z}+\frac{\partial}{\beta_{gr}\partial\tau}\right)\hat{A}_-^j-\sigma\hat{A}_-^j+i\hat{\alpha}(\hat{B}_+^j+\hat{B}_-^j)=0,$$

$$\left(\pm\frac{\partial}{\partial X}+\frac{\partial}{\beta_{gr}\partial\tau}\right)\hat{B}_\pm^j+\sigma\hat{B}_\pm^j+i\hat{\alpha}(\hat{A}_+^j+\hat{A}_-^j)=0,$$

$$\left(\frac{\partial}{\partial Z}+\frac{\partial}{\beta_\parallel\partial\tau}\right)^2\Theta=\mathrm{Re}(\hat{A}_+^j e^{i\Theta}) \tag{17a}$$

in the corrugated part of the cavity and

$$\left(\frac{\partial}{\partial Z}+\frac{\partial}{\beta_{gr}\partial\tau}\right)\hat{A}_+^0+\sigma\hat{A}_+^0=\frac{1}{\pi}\int_0^{2\pi}e^{-i\Theta}d\Theta_0,$$

$$\left(-\frac{\partial}{\partial Z}+\frac{\partial}{\beta_{gr}\partial\tau}\right)\hat{A}_-^0+\sigma\hat{A}_-^0=0 \tag{17b}$$

in the regular part of the cavity, where the subscripts $j=1,2$ refer to the first and second corrugated parts and the subscript 0 corresponds to the regular part of such a cavity. The boundary conditions for (17) take the form similar to that discussed at the beginning of this section, where the full normalized length of the resonator $L_\Sigma=l_\Sigma C\bar{k}$ should be used. To complete the set of equations (17), the continuity conditions (10) of the field at the boundaries of the different parts of the resonator must be considered.

The initial conditions for each electron in the electron beam are

$$\Theta|_{Z=0}=\Theta_0\in[0,2\pi),\quad \left(\frac{\partial}{\partial Z}+\frac{1}{\beta_\parallel}\frac{\partial}{\partial\tau}\right)\Theta\Big|_{Z=0}=\Delta, \tag{18}$$

where Θ is the electron phase with respect to the resonant wave and Θ_0 is the initial electron phase. The normalized space and time variables are $X=\bar{k}xC$, $Z=\bar{k}zC$, $\tau=\omega_0 tC$, and the normalized field amplitude is

$$\hat{A}_{\pm} = \frac{eA_{\pm}\mu\chi}{mc\omega_0\gamma_0 C^2}, \tag{19}$$

where $C=\left(\frac{eI_0\lambda}{8\pi mc^3\gamma_0}\chi^2\mu\right)^{1/3}$ is the gain parameter, $\chi \approx \beta_{\perp}/2\beta_{\parallel}$ is a constant which determines the coupling between the electrons and the wave mode, $\mu=\gamma_0^{-2}$ is the inertial bunching parameter, I_0 is the unperturbed electron current per unit transverse size, $\Delta=\left(\frac{\omega_0-\bar{k}v_{\parallel 0}-\Omega_b}{\omega_0 C}\right)$, $\hat{\alpha}=\alpha C$ is the normalized wave coupling parameter, and σ is a parameter which characterizes wave ohmic losses in the system. The electron efficiency is given by the relations

$$\eta = \frac{C}{\mu(1-\gamma_0^{-1})}\hat{\eta},$$

$$\hat{\eta} = \frac{1}{2\pi L_x}\int_0^{+L_x}\int_0^{2\pi}\left(\frac{\partial\Theta}{\partial Z}+\frac{1}{\beta_{\parallel}}\frac{\partial\Theta}{\partial Z}-\Delta\right)_{Z=L_{\Sigma}} d\Theta_0 dX, \tag{20}$$

where $L_X=l_x\bar{k}C$ is the normalized system's perimeter.

To simulate the excitation and build-up processes in the FEM based on the two-mirror cavity design the equations (17) with boundary and continuity conditions have been used under the assumption that $\beta_{\parallel}=\beta_{gr}$. Let us note that while there is a range of parameters, where single mode operation can be achieved [10], the first experiment has been designed as a proof of the concept, i.e., to observe oscillation of the FEM and to demonstrate the operation of a FEM based on 2D distributed feedback. For these purposes a cavity with 2D Bragg structures as input and output mirrors having a high-Q factor to ensure a low start current and short transition time has been designed. In this case the excitation of other modes, with frequencies located inside the mirrors' band gap, as well as relatively low FEM efficiency has been expected and observed in the simulations. The time dependency of the efficiency is presented in Fig. 11(a). The spectrum [Fig. 11(b)] of output radiation $S_{\Omega}=\int_0^{+\infty}\hat{A}_+(\tau,Z=L_{\Sigma})e^{i\Omega\tau}d\tau$ has been analyzed in the time interval from 0 ns to 300 ns. This time interval was considered to take into account the rf pulse duration observed in the experiments and to analyze the steady state operation of the FEM. It is important to note that in all the simulations carried out the transverse distribution of the amplitude of the resonant wave A_+ did not depend on the transverse coordinate x, thus providing equal energy extraction from all parts of the electron beam.

In order to tune the parameters of the FEM experiment, such as the amplitude of the guide field and the amplitude of the undulator, the 2.5 D PIC code KARAT has been used. Using this code the operation of the FEM in the self-amplification of spontaneous emission (SASE) regime was simulated. In Fig. 12(a) the electron beam transportation in the combined fields of the wiggler and the guide solenoid is presented. In this regime there is no cavity installed and the electron beam amplifies an EM wave, which meets the optimum condition for excitation [i.e., optimum field structure and satisfying the resonance condition (13)] from the initial noise signal. Therefore by varying the electron beam voltage,

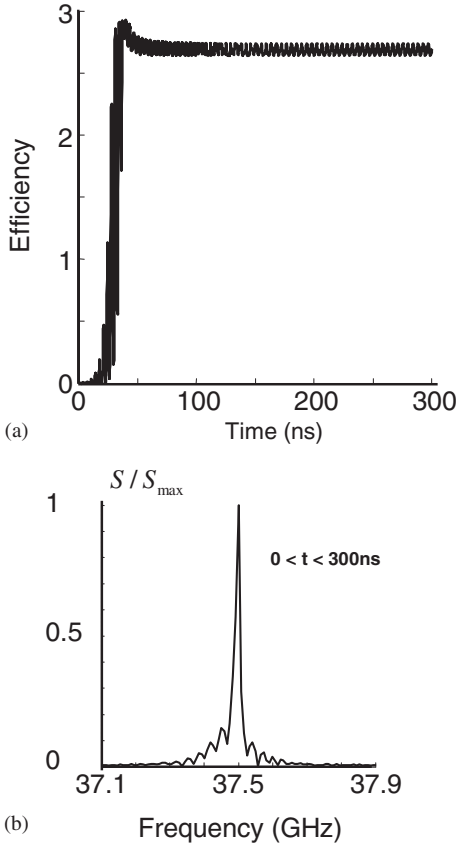

FIG. 11. The results of numerical simulation of the operation of FEM based on a 2D Bragg two-mirror cavity using the self-consistent set of equations (14) if the period of the corrugations is 0.8 cm, $\bar{m}=24$, $l_1=10$ cm, $l_2=6$ cm, $l_0=70$ cm, $\alpha=0.12$ cm^{-1}; the cavity circumference is 22 cm; the ohmic loss inside the cavity is 0.001 cm^{-1} and the gain parameter $C\sim 6\times 10^{-3}$: (a) the FEM efficiency versus time; (b) the spectrum of the output radiation in the time interval from 0 ns to 300 ns.

as well as the amplitude of the guide and undulator magnetic fields, a range of parameters where strong gain of the TEM wave at the operating frequency ~37.5 GHz was identified. Figure 12(b) shows the spectrum of the output radiation from the FEM operating in the SASE regime. These simulations were used to define a set of experimental parameters for amplification in the FEM at the 2D Bragg resonant frequency of ~37.5 GHz, as well as to define the optimum parameters of the guide field and undulator to transport the electron beam through the interaction space.

IV. HIGH POWER FEM EXPERIMENT USING 2D BRAGG COAXIAL RESONATOR

Theoretical studies of the dynamics of the coaxial FEMs based on 2D distributed feedback, together with microwave measurements with 2D structures, enabled the cavity's parameters to be chosen which minimized both the transition time and oscillation start current required. Based on the analysis of the results obtained (Fig. 9), the following parameters were obtained for the cavity: length of the input and output mirrors $l_1=10.4$ cm and $l_2=5.6$ cm, respectively,

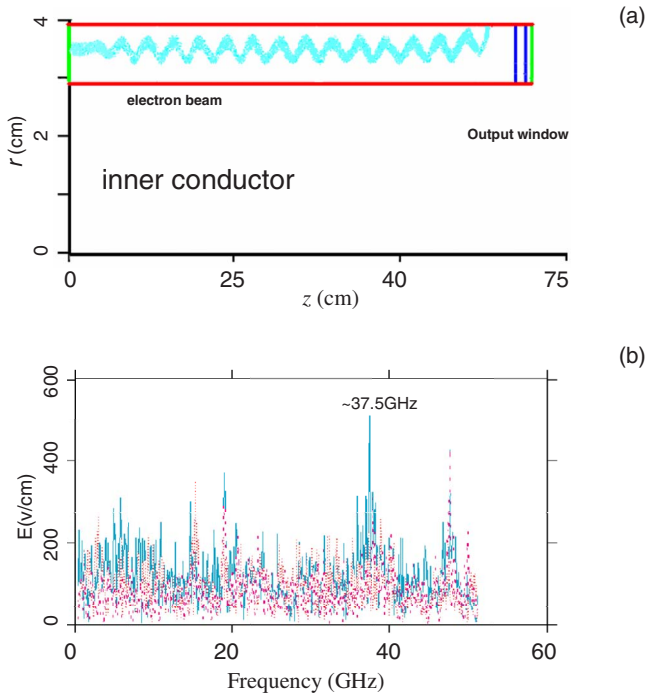

FIG. 12. (Color online) The results of the numerical simulation of the FEM in the SASE regime using the 2.5 D particle-in-cell code KARAT: (a) the electron beam (dotted, undulating thick line) transportation inside the coaxial drift tube in the combined magnetic fields of the solenoid and undulator; (b) the spectrum of the output radiation electric field components (E_r is the solid line, $E_{z,\varphi}$ are the dotted fine and bold lines, respectively).

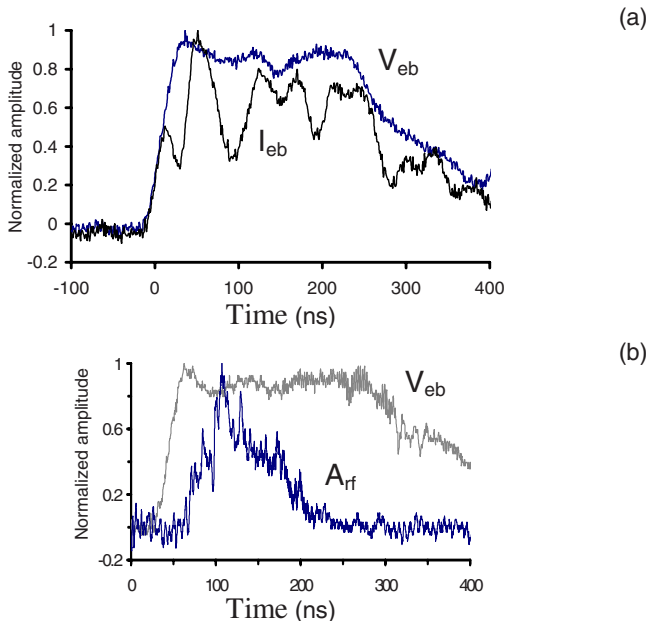

FIG. 13. (Color online) The results of the experimental study of the FEM based on the 2D Bragg two-mirror cavity and driven by the thin (2 mm) large diameter (70 mm) annular beam: (a) the traces of the electron beam accelerating voltage V_{eb} and electron beam current I_{eb}; (b) the traces of the electron beam accelerating voltage V_{eb} and output microwave pulse A_{rf}.

length of the smooth coaxial waveguide l_0=70 cm, period of corrugation of the structures 0.4 cm, and the number of the azimuthal variations of the corrugation $\bar{m}$=24. Taking into account these cavity parameters it was estimated that the transition time should not exceed 150 ns if the electron beam current exceeds 200 A.

Two-dimensional coaxial Bragg structures have been used in the FEM experiment to form the two-mirror cavity. The overlap of the band gaps (reflection zones) of these structures defines the operating frequency band of the FEM. In the experiment the central frequencies of the input and output mirrors coincided with the operating frequency range defined by the structure with the narrowest band gap, i.e., in this case by the output mirror. The results of the experimental measurements of transmission of the azimuthally symmetric TEM wave through the output (5.6 cm) mirror are presented in Fig. 8. The center of the band gap is around 37.3 GHz with the reflection coefficient −20 dB at the center frequency. The width of the band gap is associated with the wave coupling coefficient α [9–12], which depends on the structures of the coupled waves and the geometry parameters of the 2D Bragg structure. For the experiments the wave coupling coefficient was estimated to be around 0.12 cm^{-1}, if TEM waves are coupled, which corresponds to a band gap width of around ~0.4 GHz. Such structures also have band gaps associated with the coupling of other modes and the nearest band gaps are associated with coupling of forward and backward $TE_{1,0}$ and $TE_{2,0}$ waves and are located around 38 GHz and 39 GHz [11,12], respectively. Therefore, if the system parameters are optimum for excitation of one of these waves then oscillation around one of these frequencies would be expected. Due to the geometry of the supports for the inner conductor, the electron beam is divided into four sections, which makes excitation of the $TE_{2,0}$ wave more probable.

To drive the FEM a HCA based on a magnetically insulated annular plasma flare emission carbon cathode and a cylindrical anode was used [14]. A Marx bank power supply resonantly charged a deionized water-filled transmission line up to 1 MV, the output of which was switched across the cathode and anode using a high pressure spark gap, resulting in ~200 ns duration, 475 kV accelerating voltage pulse being applied across the anode and cathode in Fig. 13(a). For an accelerating voltage of 475 kV, a thin (0.2 cm) annular electron beam (~0.5 kA) of mean diameter 7.0 cm was produced and transported through the coaxial transmission line of length ~2 m, with diameters of inner and outer conductors of 6 cm and 8 cm, respectively. Mylar witness plate diagnostics were used to align the electron beam. The azimuthally symmetric undulator of period 4 cm located inside the uniform magnetic guide field was used to pump the transverse electron oscillation. The undulator field was slowly up-tapered over the initial six periods ensuring the adiabatic entrance of the electron beam inside the interaction space. The amplitude of the undulator could be varied up to 0.06 T, while the amplitude of the guide magnetic field could be varied up to 1 T. It is important to note that the two-mirror cavity was located inside the uniform part of the undulator.

In the experiments well-defined and reproducible microwave pulses were generated (with ±10% shot-to-shot varia-

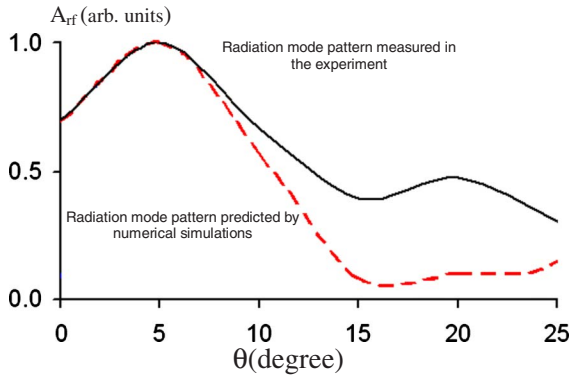

FIG. 14. (Color online) The mode pattern of the output signal from the high gain (~30 dB) coaxial horn measured in the experiment (bold line) and predicted by the 3D code MAGIC (dashed line).

tion in power and pulse width and with a constant spectrum) if the conditions were maintained the same. In Fig. 13(b) the trace of the microwave pulse in comparison with the trace of the electron beam accelerating voltage is presented. It is clearly evident that the oscillation takes place after some transition time of ~100 ns and it terminates when the electron beam voltage decreases after ~200 ns. To measure the output radiation (A_{rf}) from the FEM two Ka-band (26.5 to 40 GHz) receiving horns, with 55 dB of attenuation, in conjunction with Hewlett-Packard (HP) detectors HP8474E (0.01–50 GHz) were located at a distance of 1.5 m from the output window. The first horn was "fixed" at the same position during all the experiments to provide a reference signal. The position of the second horn was free to move and was used to study the output radiation characteristics. The output radiation pattern from a conical coaxial horn of inner and outer diameter 6 cm and 19 cm, respectively, was measured. The pattern measured in the hot experiments, when an electron beam was present, was compared with theoretical data obtained from numerical simulations using the electromagnetic solver contained within the 3D code MAGIC (Fig. 14). The output power measured at the detector was integrated over the measured radiation pattern, resulting in a FEM output power of 15 MW which corresponded to ~6% efficiency. The relative uncertainty of the power measured during the experiments did not exceed 10%.

To study the frequency of the output radiation, first a set of cutoff filters was used and it was established that the 2D Bragg FEM operated within the 36.9 GHz to 40 GHz frequency region. To study the output spectrum in more detail, the frequency of the output radiation was measured using a heterodyne frequency diagnostic. For this purpose the microwave radiation from the FEM was mixed in a nonlinear Farran Technology waveguide balanced mixer (BMC-28B). The calibration of the mixer was confirmed in the frequency range 26.5 GHz to 40 GHz in cold microwave measurements, using a 40 GHz HP synthesized sweeper acting as the local oscillator and an Anritsu pulsed sweeper which could produce a 100 ns duration millimeter wave pulse in the frequency range 0.01–50 GHz to act as the rf source to be measured. The Anritsu swept source was replaced with the output signal from the FEM. The resultant intermediate frequency captured on a deep memory, Le Croy, digitizing oscilloscope and was then analyzed. Knowing the frequency of the local oscillator (LO) and ensuring that the signal to be measured was located within a frequency of 1.5 GHz (digitizing bandwidth of the oscilloscope) from the LO, measurement of the resultant intermediate frequency enabled the output frequency of the FEM to be determined. In experiments at a local oscillator frequency of 38 GHz, the resultant intermediate frequency signal was recorded and by taking the fast Fourier transform (FFT) of the intermediate frequency signal, the spectrum of the microwave signal was plotted (Fig. 15). In Fig. 15 the traces of the microwave pulses and corresponding spectra of the microwave signals are presented. The heterodyne frequency diagnostic was used to study frequency tuning of the 2D Bragg FEM as the undulator and solenoid magnetic field were varied. By tuning the amplitude of the guide magnetic field and the undulator field two frequency regions around 37.2 GHz and 39.4 GHz associated with the frequency bands of the 2D structures were measured. When the amplitude of the undulator field was large enough to produce electrons with a pitch factor of ~0.17 the excitation of the TEM azimuthally symmetric mode associated with the first band gap of the structure (37.0–37.4 GHz) was observed (Fig. 15, first column). Decrease of the undulator field, i.e., the decrease of the pitch factor, resulted in an up-shift of the operating frequency into the region associated with the second band gap at 39.3–39.6 GHz associated with excitation of the first azimuthally nonsymmetric wave $TE_{2,0}$ (Fig. 15, second column). The presence of the $TE_{2,0}$ mode can be partially explained by the geometry of the system because the presence of the symmetric supports of the inner conductor effectively divide the beam into four sectors. Further decrease of the undulator field leads to the disappearance of the microwave signal. In all the experiments a single spectral line above the pedestal was observed. It should be noted that the pedestal width correlated well with the width of the band gap. The lines of reduced amplitude adjacent to the main spectral line, clearly evident in Fig. 15, may be associated with the transition processes inside the cavity.

V. CONCLUSION

In this paper the results have been presented of theoretical and experimental studies of a FEM based on 2D distributed feedback. The results achieved at each step of the FEM experiment have been reported. The lasing of a FEM based on 2D distributed feedback and driven by an oversized annular electron beam has been observed. In the paper it has been demonstrated theoretically and confirmed experimentally that 2D Bragg structures can be used as highly reflective narrow band, mode selective, mirrors with effective band gaps defined by the corrugation depths and lengths of the structures. It has been theoretically and experimentally shown that a two-mirror cavity based on such a 2D Bragg structure having high selective properties can be used in high-power masers driven by an oversized electron beam. Using the results of the theoretical studies and data from measurements of the 2D Bragg structures, the new two-mirror cavity has been designed and constructed. In these

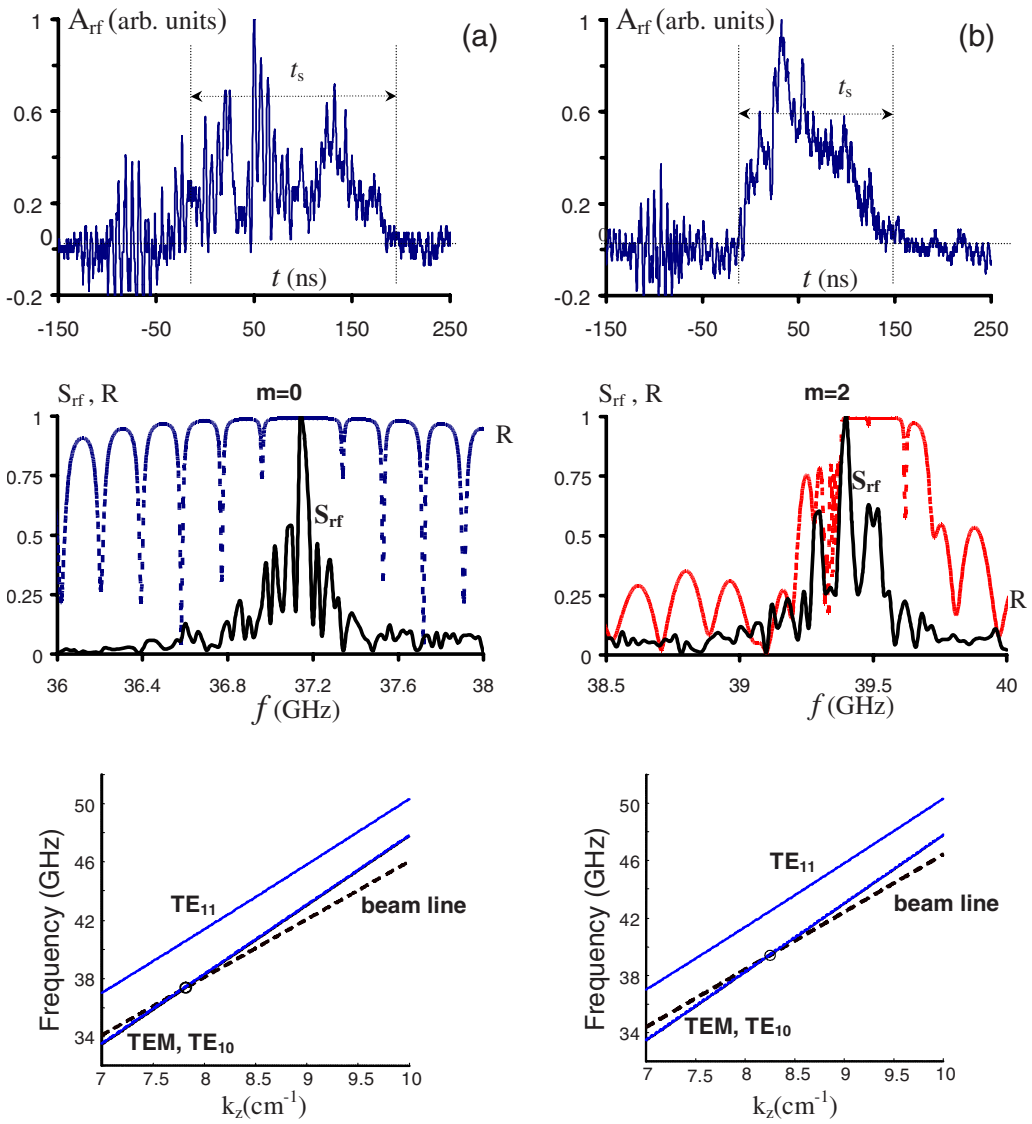

FIG. 15. (Color online) The output traces of the microwave pulses (first row), (second row) their spectra (solid line) and cavity reflection coefficients (dotted lines) for $m=0$ and $m=2$, (third row) waves' dispersions (solid lines) with the electron beam line (dashed line) illustrating the wave-beam resonance condition for different values of guide and undulator magnetic fields: column (a) guide magnetic field is 0.6 T and amplitude of undulator field is 0.06 T; column (b) guide magnetic field is 0.5 T and amplitude of undulator field is 0.03 T.

first experiments a high-Q cavity was used, which restricted the efficiency. Decreasing the cavity Q factor, in accordance with numerical simulations, should result in an increase in efficiency, which will be the next goal of the future experiments. Also, the possibility of using a one-dimensional Bragg structure as an output mirror has been discussed in the previous work [15] and it will be used in the future experiments to improve the EM field structure inside the interaction space, to reduce the ohmic losses, and thus to improve the FEM efficiency.

The operation of the FEM was observed in two different frequency regions, which are well defined by the band gap parameters of the 2D periodic structures used as input and output mirrors of the two-mirror cavity. In the experiments a TEM wave mode pattern from the output horn was observed, with a measured output power of ~15 MW, which corresponds to ~6% efficiency. The results obtained correspond well with the theoretical predictions made in previous work. Experimental operation of the coaxial 2D Bragg FEM demonstrates the proof of the concept, namely that an oversized active device with 2D distributed feedback can be used to achieve mode selection over the transverse index. The results are relevant to several other branches of physics, including integrated optics, photonics, and signal processing where distributed feedback is widely used [16–18].

ACKNOWLEDGMENTS

The authors would like to thank EPSRC, QinetiQ, PPARC/STFC, and the Faraday Partnership in High-Power RF for partial support of this work. One of the authors (P.M.) would like to thank PPARC/STFC and the University of Strathclyde for support.

[1] Evgenya I. Smirnova, Amit S. Kesar, Ivan Mastovsky, Michael A. Shapiro, and Richard J. Temkin, Phys. Rev. Lett. **95**, 074801 (2005).
[2] J. R. Sirigiri, M. A. Shapiro, and R. J. Temkin, Phys. Rev. Lett. **90**, 258302 (2003).
[3] N. S. Ginzburg, A. A. Kaminsky, A. K. Kaminsky, N. Yu. Peskov, S. N. Sedykh, A. P. Sergeev, and A. S. Sergeev, Phys. Rev. Lett. **84**, 3574 (2000).
[4] W. P. Leemans, C. G. R. Geddes, J. Faure, Cs. Tóth, J. van Tilborg, C. B. Schroeder, E. Esarey, G. Fubiani, D. Auerbach, B. Marcelis, M. A. Carnahan, R. A. Kaindl, J. Byrd, and M. C. Martin, Phys. Rev. Lett. **91**, 074802 (2003); W. P. Leemans, J. van Tilborg, J. Faure, C. G. R. Geddes, Cs. Tóth, C. B. Schroeder, E. Esarey, G. Fubiani, and G. Dugan, Phys. Plasmas **11**, 2899 (2004); Zheng-Ming Sheng, Kunioki Mima, and Jie Zhang, *ibid.* **12**, 123103 (2005).
[5] S. E. Korbly, A. S. Kesar, J. R. Sirigiri, and R. J. Temkin, Phys. Rev. Lett. **94**, 054803 (2005).
[6] Yu. A. Grishin, M. R. Fuchs, A. Schnegg, A. A. Dubinskii, B. S. Dumesh, F. S. Rusin, V. L. Bratman, and K. Möbius, Rev. Sci. Instrum. **75**, 2926 (2004).
[7] N. S. Ginzburg, N. Yu. Peskov, and A. S. Sergeev, Opt. Commun. **112**, 151 (1994).
[8] N. S. Ginzburg, A. S. Sergeev, N. Yu. Peskov, G. R. M. Robb, and A. D. R. Phelps, IEEE Trans. Plasma Sci. **24**, 770 (1996).
[9] N. S. Ginzburg, N. Yu. Peskov, A. S. Sergeev, A. D. R. Phelps, I. V. Konoplev, G. R. M. Robb, A. W. Cross, A. V. Arzhannikov, and S. L. Sinitsky, Phys. Rev. E **60**, 935 (1999).
[10] N. S. Ginzburg, N. Yu. Peskov, A. S. Sergeev, I. V. Konoplev, A. W. Cross, A. D. R. Phelps, G. R. M. Robb, K. Ronald, W. He, and C. G. Whyte, J. Appl. Phys. **92**, 1619 (2002); A. W. Cross, W. He, I. V. Konoplev, A. D. R. Phelps, K. Ronald, G. R. M. Robb, C. G. Whyte, N. S. Ginzburg, N. Yu. Peskov, and A. S. Sergeev, Nucl. Instrum. Methods Phys. Res. A **475**, 164 (2001).
[11] A. W. Cross, I. V. Konoplev, A. D. R. Phelps, and K. Ronald, J. Appl. Phys. **93**, 2208 (2003); I. V. Konoplev, A. D. R. Phelps, A. W. Cross, and K. Ronald, Phys. Rev. E **68**, 066613 (2003).
[12] A. W. Cross, I. V. Konoplev, K. Ronald, A. D. R. Phelps, W. He, C. G. Whyte, N. S. Ginzburg, N. Yu. Peskov, and A. S. Sergeev, Appl. Phys. Lett. **80**, 1517 (2002).
[13] A. F. Harvey, *Microwave Engineering* (Academic, London, 1963).
[14] I. V. Konoplev, A. W. Cross, P. MacInnes, W. He, C. G. Whyte, A. D. R. Phelps, C. W. Robertson, K. Ronald, and A. R. Young, Appl. Phys. Lett. **89**, 171503 (2006); J. A. Nation, *ibid.* **17**, 491 (1970); M. Friedman, J. Pasour and D. Smithe, *ibid.* **71**, 3724 (1997).
[15] N. S. Ginzburg, N. Yu. Peskov, A. S. Sergeev, A. D. R. Phelps, A. W. Cross, and I. V. Konoplev, Phys. Plasmas **9**, 2798 (2000).
[16] E. Yablonovitch, Phys. Rev. Lett. **58**, 2059 (1987).
[17] S. Fan, P. R. Villeneuve, J. D. Joannopoulos, and H. A. Haus, Phys. Rev. Lett. **80**, 960 (1998).
[18] S. G. Johnson, S. Fan, P. R. Villeneuve, J. D. Joannopoulos, and L. A. Kolodziejski, Phys. Rev. B **60**, 5751 (1999).